Glycoside hydrolase family 18 and 20 enzymes are novel targets of the traditional medicine berberine

Received for publication, June 7, 2018, and in revised form, August 3, 2018 Published, Papers in Press, August 22, 2018, DOI 10.1074/jbc.RA118.004351

Yanwei Duan[‡], **Tian Liu**[‡1], **Yong Zhou**[‡], **Tongyi Dou**[§], **and Qing Yang**[‡¶2]

From the [‡]*State Key Laboratory of Fine Chemical Engineering, School of Life Science and Biotechnology and School of Software, Dalian University of Technology, Dalian 116024, the* [§]*School of Life Science and Medicine, Dalian University of Technology, Panjin 124221, and the* [¶]*Institute of Plant Protection, Chinese Academy of Agricultural Sciences, Beijing 100193, China*

Edited by Gerald W. Hart

Berberine is a traditional medicine that has multiple medicinal and agricultural applications. However, little is known about whether berberine can be a bioactive molecule toward carbohydrate-active enzymes, which play numerous vital roles in the life process. In this study, berberine and its analogs were discovered to be competitive inhibitors of glycoside hydrolase family 20 β-*N*-acetyl-D-hexosaminidase (GH20 Hex) and GH18 chitinase from both humans and the insect pest *Ostrinia furnacalis*. Berberine and its analog SYSU-1 inhibit insect GH20 Hex from *O. furnacalis* (*Of*Hex1), with K_i values of 12 and 8.5 μM, respectively. Co-crystallization of berberine and its analog SYSU-1 in complex with *Of*Hex1 revealed that the positively charged conjugate plane of berberine forms π–π stacking interactions with Trp^{490}, which are vital to its inhibitory activity. Moreover, the 1,3-dioxole group of berberine binds an unexplored pocket formed by Trp^{322}, Trp^{483}, and Val^{484}, which also contributes to its inhibitory activity. Berberine was also found to be an inhibitor of human GH20 Hex (*Hs*HexB), human GH18 chitinase (*Hs*Cht and acidic mammalian chitinase), and insect GH18 chitinase (*Of*ChtI). Besides GH18 and GH20 enzymes, berberine was shown to weakly inhibit human GH84 *O*-GlcNAcase (*Hs*OGA) and *Saccharomyces cerevisiae* GH63 α-glucosidase I (*Sc*GluI). By analyzing the published crystal structures, berberine was revealed to bind with its targets in an identical mechanism, namely via π–π stacking and electrostatic interactions with the aromatic and acidic residues in the binding pockets. This paper reports new molecular targets of berberine and may provide a berberine-based scaffold for developing multitarget drugs.

Berberine is an isoquinoline quaternary alkaloid widely distributed in the root, stem, and bark of plants from the Berberis and Coptis families, such as *Berberis aristata*, *Berberis aquifolium*, *Berberis vulgaris*, *Coptis chinesis*, *Coptis japonica,* and *Coptis rhizome* (1–3). Berberine has been used for more than 3,000 years in Ayurvedic, Chinese, and Middle-Eastern folk medicine for its antimicrobial, antiprotozoal, antidiarrheal, and antitrachomatic activities (1–3). With the development of modern biomedicine, berberine has been revealed to have a very wide range of pharmacological properties, including anticancer, antidiabetic, antidepressant, antihyperlipidemic, and antihypertensive activities (4–8). Moreover, berberine has also been revealed to have potential applications in agriculture for its antifungal, insecticidal, and herbicidal activities (9–11). Corresponding to its multispectrum activities, several molecular targets of berberine, such as glycogen synthase kinase, calmodulin kinase, matrix metalloprotease, acetylcholinesterase, butyrylcholinesterase, monoamine oxidase, DNA topoisomerase, cyclin, and transcriptional factor p53 (12–18), have been discovered.

Glycoside hydrolase family 20 β-*N*-acetyl-D-hexosaminidase (GH20 Hex)[3] catalyzes the removal of *N*-acetyl-D-glucosamine (GlcNAc) or *N*-acetyl-D-galactosamine (GalNAc) from various glycans, glycolipids, and glycoproteins (19, 20). Insect Hex has been proven to be vital for the survival of agricultural pests (21–26). Human Hex is also important for health. Dysfunction of human Hex results in lysosomal storage diseases and osteoarthritis (27, 28). Glycoside hydrolase family 18 (GH18) chitinase not only catalyzes chitin degradation in bacteria, fungi, and insects but also plays different roles in other organisms (29). For example, human chitinases (*Hs*Cht and AMCase) have been reported to be involved in asthma (30) and other immunological disorders (31–33). Chitinases from parasites causing nematodosis (34) and malaria (35) are also important for the development and pathogenesis of these organisms. In view of the abovementioned roles of GH20 Hexs and chitinases, inhibitors targeting these enzymes are potential therapeutic agents and agrochemicals (36–39). Glycoside hydrolase family 84 *O*-GlcNAcase (*Hs*OGA) removes *O*-linked GlcNAc (*O*-GlcNAc)

This work was supported by the Program for National Natural Science Funds for Distinguished Young Scholar (Grant 31425021) and the National Natural Science Foundation of China (Grants 31830076 and 31871959). The authors declare that they have no conflicts of interest with the contents of this article.

The atomic coordinates and structure factors (codes 5Y0V and 5Y1B) have been deposited in the Protein Data Bank (http://wwpdb.org/).

[1] To whom correspondence may be addressed. Tel.: 86-411-84707245; Fax: 86-411-84707245; E-mail: tianliu@dlut.edu.cn.

[2] To whom correspondence may be addressed. Tel.: 86-411-84707245; Fax: 86-411-84707245; E-mail: qingyang@dlut.edu.cn.

[3] The abbreviations used are: GH20 Hex, glycoside hydrolase family 20 β-*N*-acetyl-D-hexosaminidase; AMCase, acidic mammalian chitinase; GH18, glycoside hydrolase family 18; GH84, glycoside hydrolase family 84; GH63, glycoside hydrolase family 63; GH13, glycoside hydrolase family 13; GlcNAc, *N*-acetyl-D-glucosamine; Hex, *Hs*Cht, human chitotriosidase; *Hs*HexB, human β-*N*-acetyl-D-hexosaminidase B; MU-β-GlcNAc, 4-methylumbelliferyl-β-*N*-acetyl-D-glucosamine; MU–α-glucose, 4-methylumbelliferyl α-D-glucopyranoside; *Of*ChtI, group I chitinase from *O. furnacalis*; *Of*Hex1, group I β-*N*-acetyl-D-hexosaminidase from *O. furnacalis*; *Hs*OGA, *O*-GlcNAcase from human; *Sc*GluI, α-glucosidase I from *S. cerevisiae*; PPA, porcine pancreatic α-amylase; bis-tris, 2-[bis(2-hydroxyethyl)amino]-2-(hydroxymethyl)propane-1,3-diol.

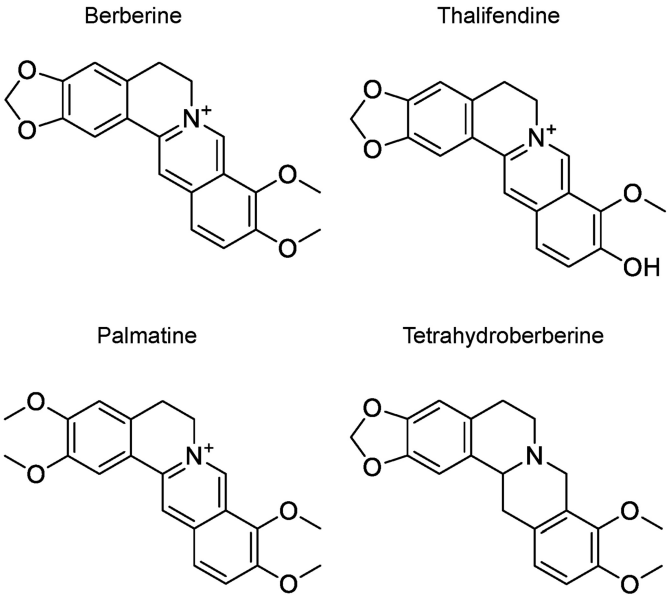

Figure 1. Structure of berberine and its analogs.

from nucleocytoplasmic proteins that are involved in transcriptional regulation and stress response (40). Glycoside hydrolase family 63 α-glucosidase I (GluI) is a key member of the eukaryotic *N*-glycosylation-processing pathway. Inhibition of GluI activity decreases infectivity of several enveloped viruses, including hepatitis B and C (41).

In the previous work, we noticed that compounds with a large conjugated plane were highly potent inhibitors of GH20 Hex (21, 42) and GH18 chitinase (39). Berberine is a typical compound with a large conjugated plane. Here, we report that berberine and its analogs (Fig. 1) act as inhibitors of GH20, GH18, GH84, and GH63 enzymes. The inhibition mechanism of berberine for these enzymes was revealed by crystallography and molecular docking. By comparison with published structures, berberine was revealed to have a similar inhibition mechanism for these structurally and functionally diverse proteins. This work provides the first report of berberine targeting glycoside hydrolases.

Results

Inhibition of GH20, GH18, GH84, GH63, and GH13 enzymes by berberine and its analogs

SYSU-1 is a berberine derivative originally reported as a telomeric G-quadruplex DNA-stabilizing ligand (43). In our preliminary screening, SYSU-1 was found to display an inhibition rate of 58.7% against *Of*Hex1, an insect GH20 member, at a concentration of 10 μM. In this study, the K_i value of SYSU-1 for *Of*Hex1 was determined to be 8.5 μM (Fig. 2). Then, the inhibitory activities of berberine itself against *Of*Hex1 as well as *Hs*HexB, a human GH20 member, were studied. Inhibition kinetics demonstrated that berberine inhibits both *Of*Hex1 and *Hs*HexB in a competitive mode, but the K_i value of berberine for *Hs*HexB was 20-fold higher than that of berberine against *Of*Hex1 (Fig. 2 and Table 1). Berberine analogs, including thalifendine and palmatine, were also found to be inhibitors of *Of*Hex1 and *Hs*HexB, and they all showed ~5-fold higher K_i values for *Hs*HexB than for *Of*Hex1 (Fig. 2 and Table 1). However, tetrahydroberberine did not inhibit *Of*Hex1 and *Hs*HexB at the concentration of 100 μM (its solubility limit in 2% DMSO).

To evaluate whether berberine can act as a scaffold for developing an inhibitor for a broad spectrum of glycosyl hydrolases, the inhibitory activities of berberine and its analogs toward GH18, GH84, GH63, and GH13 enzymes were assayed, and the K_i values were determined. Berberine, thalifendine, and palmatine showed inhibitory activities against GH18, GH84, and GH63 enzymes in a competitive mode, but it did not inhibit GH13 porcine pancreatic α-amylase (PPA) even at a concentration of 400 μM. Tetrahydroberberine did not inhibit all these enzymes at the concentration of 100 μM (Figs. 3 and 4 and Table 1). In addition, berberine and its analogs showed moderate selectivity between two human chitinases. They had 3–5-fold higher K_i values for AMCase than for *Hs*Cht.

Crystal structure of OfHex1 in complex with berberine

To reveal the inhibition mechanism of berberine against *Of*Hex1, the complexed structure of *Of*Hex1 and berberine was prepared by soaking and was resolved to a solution of 2.4 Å. The statistics of data collection and structure refinement are shown in Table 2. The coordinates of the *Of*Hex1–berberine complex and OfHex1–SYSU-1 complex have been deposited in the Protein Data Bank under accession numbers 5Y0V and 5Y1B.

The electron-density map supports the location of berberine in the active pocket of *Of*Hex1 (Fig. 5*A*). Berberine binds *Of*Hex1 across the −1 and +1 subsites mainly via a π–π stacking interaction with Trp^{490} and van der Waals interactions with the surrounding residues (Fig. 5, *B* and *C*). The positive charge of berberine can be neutralized by the negative electrostatic potential in the active pocket (Fig. 5*B*). Trp^{490} appears to be important for berberine's binding because it forms a π–π stacking interaction with the berberine ring and a water-mediated hydrogen bond with the O1 of berberine. The mutant *Of*Hex1–W490A was not inhibited by berberine at 100 μM (data not shown). Moreover, a hydrophobic recess composed of Trp^{322}, Trp^{483}, and Val^{484} also contributed to the binding of berberine by accommodating its 1,3-dioxole group (Fig. 5). Palmatine without the 1,3-dioxole group showed a K_i value for *Of*Hex1 that was more than 4-fold higher than that of berberine (Table 1). Notably, this hydrophobic recess has not been occupied by other *Of*Hex1 inhibitors, such as *N,N,N*-trimethyl-D-glucosaminyl-chitotriomycin (TMG-chitotriomycin) (44), *N*-acetylglucosaminono-1,5-lactone *O*-(phenylcarbamoyl)-oxime (PUGNAc) (45), 3*aR*,5*R*,6*S*,7*R*,7*aR*)-5-(hydroxymethyl)-2-methyl-5,6,7,7*a*-tetrahydro-3aH-pyrano[3,2-*d*]thiazole-6,7-diol (NAG-thiazoline) (46), 2-(2-(((5-methyl-1,3,4-thiadiazol-2-yl)methyl)amino)ethyl)-1*H*-benzo[de]isoquinoline-1,3(2*H*)-dione (Q1), and 6-(dimethylamino)-2-(2-(((5-methyl-1,3,4-thiadiazol-2-yl)methyl)amino)ethyl)-1*H*-benzo[de]isoquinoline-1,3(2*H*)-dione (Q2) (42).

Crystal structure of OfHex1 in complex with SYSU-1

The complexed structure of *Of*Hex1 and SYSU-1 was also prepared by soaking and was resolved to a solution of 2.2 Å. The statistics of data collection and structure refinement are shown

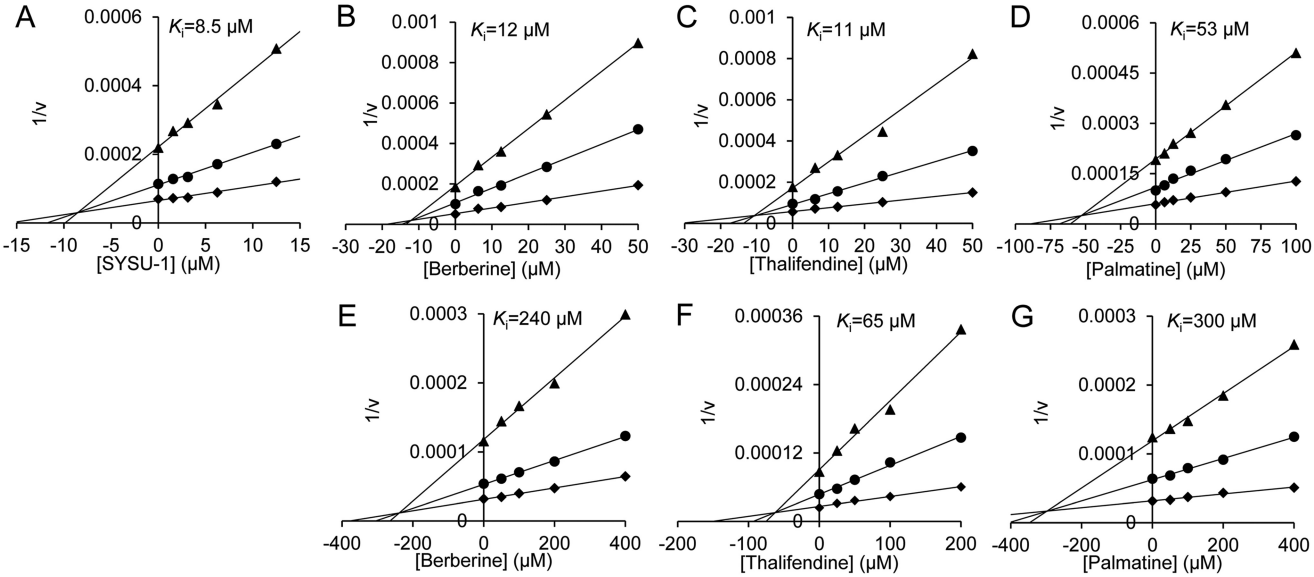

Figure 2. Inhibition kinetics of berberine and its analogs toward GH20 Hexs. *A*, inhibition kinetics of SYSU-1 toward *Of*Hex1; *B* and *E*, inhibition kinetics of berberine toward *Of*Hex1 and *Hs*HexB; *C* and *F*, inhibition kinetics of thalifendine toward *Of*Hex1 and *Hs*HexB; and *D* and *G*, inhibition kinetics of palmatine toward *Of*Hex1 and *Hs*HexB.

Table 1
K_i values of berberine and its analogs against GH20 and GH18 enzymes

	K_i (μM)							
	GH20		GH18					
Compound	*Of*Hex1	*Hs*HexB	*Of*ChtI	*Hs*Cht	AMCase	GH84, *Hs*OGA	GH63, *Sc*GluI	GH13, PPA
Berberine	12	240	23	19	65	118	130	NI[a]
Thalifendine	11	65	15	15	55	72	74	NI[a]
Palmatine	53	300	38	15	70	194	600	NI[a]
Tetrahydroberberine	NI[b]	NI[b]	NI[b]	NI[b]	NI[b]	NI[b]	NI[b]	NI[b]

[a] NI indicates not inhibited at a concentration of 400 μM.
[b] NI indicates not inhibited at a concentration of 100 μM.

in Table 2. The coordinates and the *Of*Hex1-SYSU-1 complex have been deposited into the Protein Data Bank under accession number 5Y1B.

The electron-density map of the berberine ring of SYSU-1 is clear and supports the binding of SYSU-1 in the active pocket of *Of*Hex1 (Fig. 6*A*). Superimposition of the complex structures of *Of*Hex1–SYSU-1 and *Of*Hex1–berberine revealed that the binding mode of the berberine moiety of SYSU-1 in *Of*Hex1 is identical to that of berberine (Fig. 6*B*). Most of the residues in the active pockets that interacted with the ligand were in the same conformation except Trp^{448}, which was rotated ~10° outward from the center of the active pocket. The electron density for the 1-butylquinolin-1-ium group of SYSU-1 is not clear, indicating disorder in this region. Nevertheless, the 1-butylquinolin-1-ium group as well as the linker region may enhance the binding affinity of SYSU-1 via van der Waals interactions or π–π stacking interactions with the surrounding aromatic residues, such as Trp^{448} and Tyr^{471} (Fig. 6*B*).

Modeled structures of other GH20, GH18, GH84, GH63, and GH13 enzymes in complex with berberine

The binding mode of berberine to *Hs*HexB was studied by the molecular docking of berberine to the crystal structure of *Hs*HexB (47). As shown in Figs. 6*B* and 7*A*, berberine could be only partially inserted into the active pocket and formed a π–π stacking interaction with Trp^{489}. Compared with berberine binding to *Of*Hex1, berberine bound to *Hs*HexB is more solvent-exposed, which may weaken the hydrophobic interaction with the active-site residues. Moreover, the positive charge of berberine may be repulsed by the positive electrostatic potential in the active pocket (Fig. 7*A*).

The binding modes of berberine to *Hs*Cht, *Of*ChtI, and AMCase were studied by molecular docking (Fig. 7, *C–F*). The results demonstrated that berberine was placed into an identical position in the substrate-binding clefts of these chitinases by forming π–π stacking interactions with a conserved tryptophan residue (Fig. 7*F*). Although the electrostatic potentials in the active pockets of these chitinases are from negative to neutral (Fig. 7, *C–E*), the positive charge of berberine might be neutralized by a conserved aspartate residue (Fig. 7*F*).

The binding modes of berberine to *Hs*OGA, *Sc*GluI, and PPA were also studied by molecular docking (Fig. 8). As the electrostatic potentials in the active pockets of *Hs*OGA and *Sc*GluI are negative, the positive charge of berberine might be neutralized by the surrounding negatively charged residues (Fig. 8, *A* and *B*). As for PPA, although berberine could be docked into the wide active pocket of PPA, it could not form any π–π stacking interactions or electrostatic interactions with PPA (Fig. 8*C*).

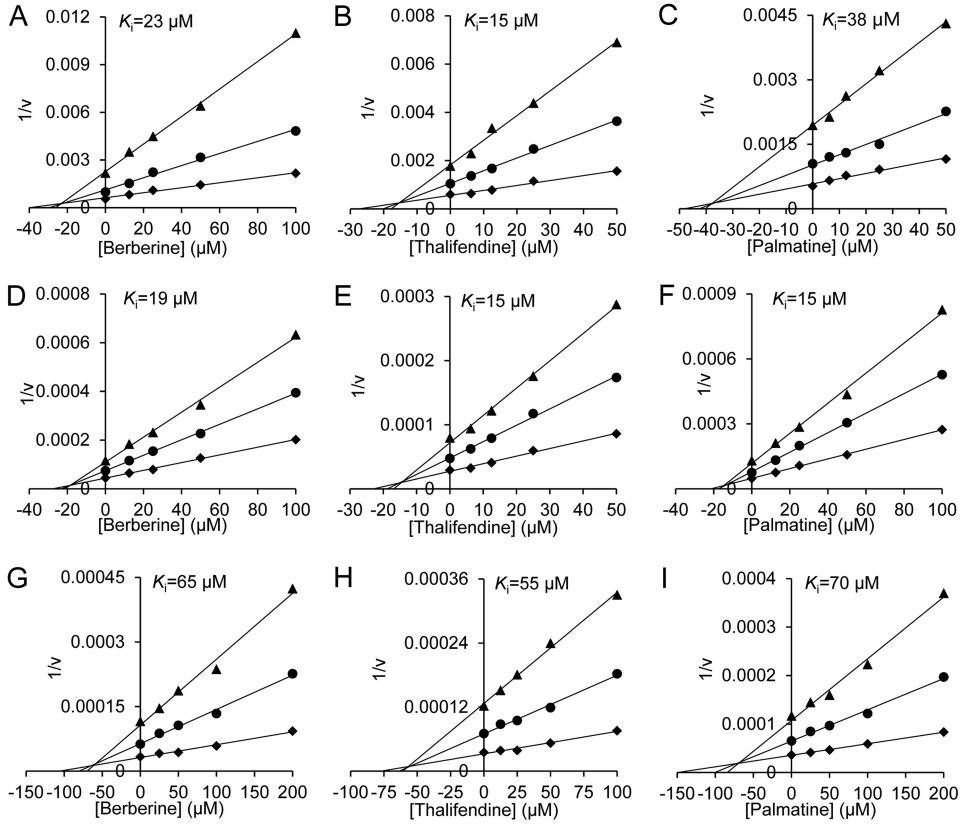

Figure 3. Inhibition kinetics of berberine and its analogs toward GH18 chitinases. *A, D,* and *G*, inhibition kinetics of berberine toward *Of*ChtI, *Hs*Cht, and AMCase; *B, E,* and *H*, inhibition kinetics of thalifendine toward *Of*ChtI, *Hs*Cht, and AMCase; and *C, F,* and *I*, inhibition kinetics of palmatine toward *Of*ChtI, *Hs*Cht, and AMCase.

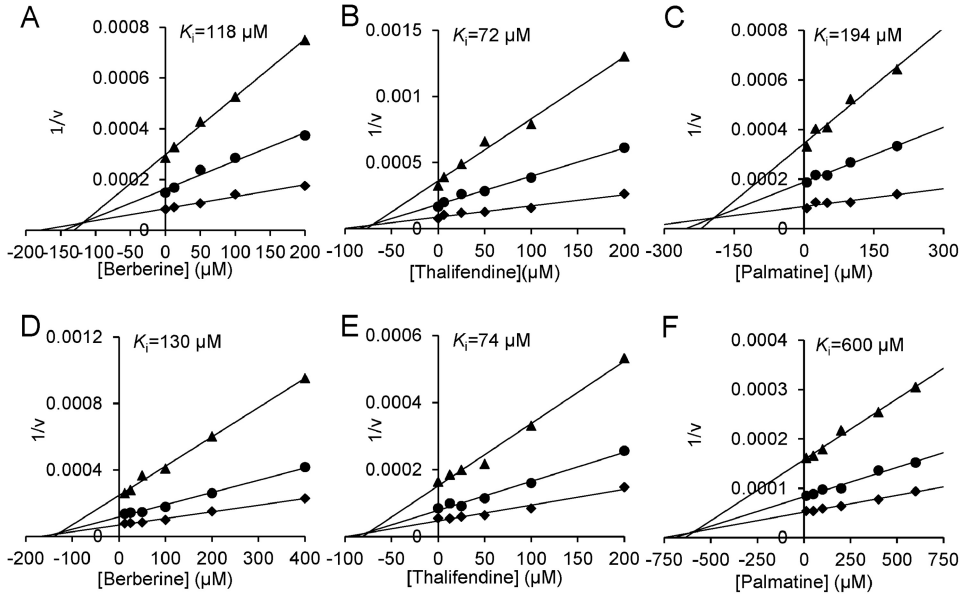

Figure 4. Inhibition kinetics of berberine and its analogs toward GH84 and GH63 enzymes. *A* and *D*, inhibition kinetics of berberine toward *Hs*OGA and *Sc*GluI; *B* and *E*, inhibition kinetics of thalifendine toward *Hs*OGA and *Sc*GluI; and *C* and *F*, inhibition kinetics of palmatine toward *Hs*OGA and *Sc*GluI.

In vivo activity of berberine and SYSU-1

To test their bioactivity, the artificial diet that contained berberine and SYSU-1, respectively, was used to feed 4th-instar day 1 *Ostrinia furnacalis* larvae. Compared with the control group, compounds fed larvae grew slowly, and some of them died after 6 days (Fig. 9).

Discussion

In this study, berberine was discovered to be a competitive inhibitor of GH20 and GH18 enzymes. Similar to the amylase inhibitor montobretin A (48), berberine binds with the target enzymes by a noncanonical mode that is not the binding mode of the transition state analog inhibitor or a substrate.

Table 2
Details of data collection and structure refinement

	*Of*Hex1–berberine	*Of*Hex1–SYSU-1
Space group	$P3_221$	$P3_221$
Unit-cell parameters		
a (Å)	107.821	107.983
b (Å)	107.821	107.983
c (Å)	175.098	175.529
Wavelength (Å)	0.97775	0.97853
Temperature (K)	100	100
Resolution (Å)	32.79–2.423 (2.51–2.423)	19.46–2.207 (2.286–2.207)
Unique reflections	41,233 (2260)	57,623 (3959)
Observed reflections	82,312 (4513)	115,092 (7911)
R_{merge}	0.129 (0.4719)	0.09773 (0.3229)
Average multiplicity	2.0 (2.0)	2.0 (2.0)
$\langle I/\sigma(I)\rangle$	21.55 (8.73)	24.01 (9.84)
Completeness (%)	90.62 (50.28)	95.63 (66.59)
R/R_{free}	0.1787/0.2026	0.1713/0.1918
Protein atoms	4615	4615
Water molecules	230	517
Other atoms	67	65
Root mean square deviation from ideal		
Bond lengths (Å)	0.003	0.003
Bond angles (°)	0.570	0.610
Wilson *B* factor (Å^2)	35.06	28.21
Average *B* factor (Å^2)	40.95	33.06
Protein atoms	40.37	31.77
Water molecules	41.41	40.54
Ramachandran plot (%)		
Favored	96.49	97.54
Allowed	3.51	2.28
Outliers	0.00	0.18
PDB code	5Y0V	5Y1B

As revealed by X-ray crystallography as well as molecular docking, berberine inhibits these enzymes via an identical mechanism. As a positively charged conjugate plane, berberine usually binds in a narrow pocket with negative electrostatic potential and forms $\pi-\pi$ stacking interactions with a conserved tryptophan residue (Trp^{490} in *Of*Hex1, Trp^{489} in *Hs*HexB, Trp^{99} in *Hs*Cht, Trp^{99} in AMCase, and Trp^{107} in *Of*ChtI) (Figs. 5*B* and 7, *A* and *B*) and electrostatic interactions with a conserved negatively charged residue (Glu^{328} in *Of*Hex1, Glu^{491} in *Hs*HexB, Asp^{213} in *Hs*Cht, Asp^{213} in AMCase, Asp^{218} in *Of*ChtI, Asp^{175} in *Hs*OGA, and Glu^{771} in *Sc*GluI) (Figs. 5*B*, 7, *A* and *B*, and 8). To determine whether berberine binds other known target proteins by the same mechanism, the reported complexed structures of berberine with other protein targets were analyzed. These protein targets included the multidrug binding protein QacR from *Staphylococcus aureus* (49), the multidrug resistance regulator BmrR from *Bacillus subtilis* (50), and RamR from *Salmonella typhimurium* (51). Although the structures and functions of these proteins vary greatly, we observed that berberine binds these proteins in a similar mode to that observed with GH20 and GH18 enzymes (Fig. 10). The conjugate plane of berberine formed $\pi-\pi$ stacking interactions with aromatic residues (Trp^{61}, Tyr^{93}, Tyr^{123} in QacR; Phe^{224}, Tyr^{229}, and Tyr^{268} in BmrR; Phe^{155} in RamR). Moreover, the positive charge of berberine could be neutralized by the surrounding

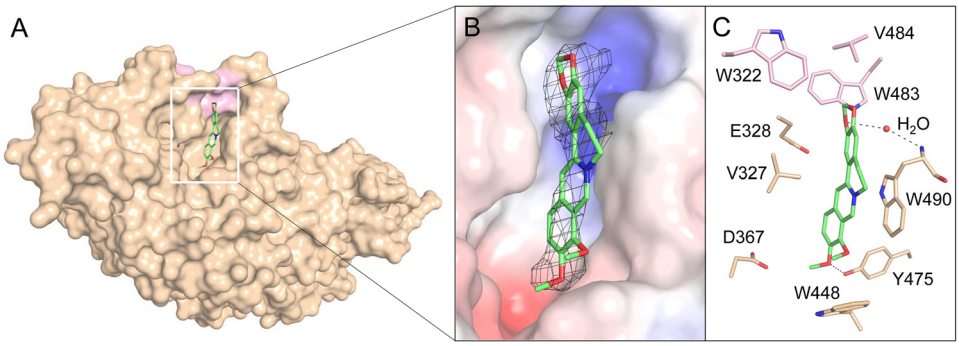

Figure 5. Crystal structures of *Of*Hex1 in complex with berberine. *A*, surface representations of *Of*Hex1 complexed with berberine. *B*, binding mode of berberine in the active pocket of *Of*Hex1. Electrostatic potential between −6 *kT/e* and 6 *kT/e* was shown as a colored gradient from *red* (acidic) to *blue* (basic). The $2F_o - F_c$ electron-density map around the ligand is contoured at the 1.0 σ level. *C*, amino acid residues involved in the binding of berberine in the active pocket of *Of*Hex1. The hydrophobic recess accommodating the 1,3-dioxole group of berberine is shown in *pink*. The hydrogen bonds are shown as *dashed black lines*.

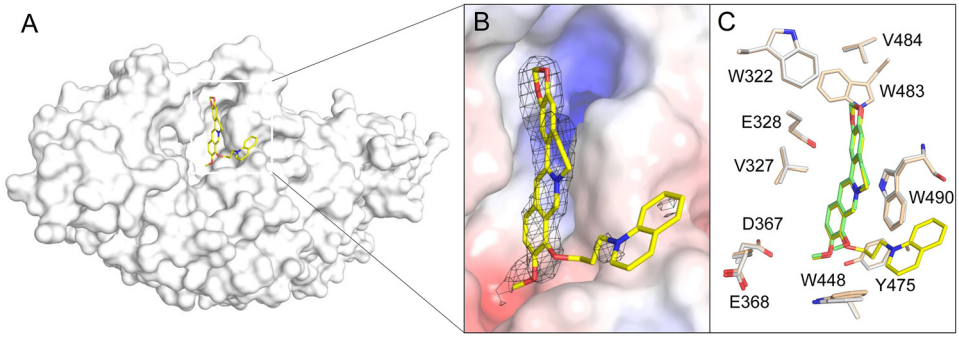

Figure 6. Crystal structures of *Of*Hex1 in complex with SYSU-1. *A*, surface representations of *Of*Hex1 complexed with SYSU-1. *B*, binding mode of SYSU-1 in the active pocket of *Of*Hex1. Electrostatic potential between −6 *kT/e* and 6 *kT/e* was shown as a colored gradient from *red* (acidic) to *blue* (basic). The $2F_o - F_c$ electron-density map around the ligand is contoured at the 1.0 σ level. *C*, superimposition of the berberine-complexed and SYSU-1–complexed *Of*Hex1. Residues of the berberine-complexed and SYSU-1–complexed *Of*Hex1 are shown in *wheat* and *white*, respectively.

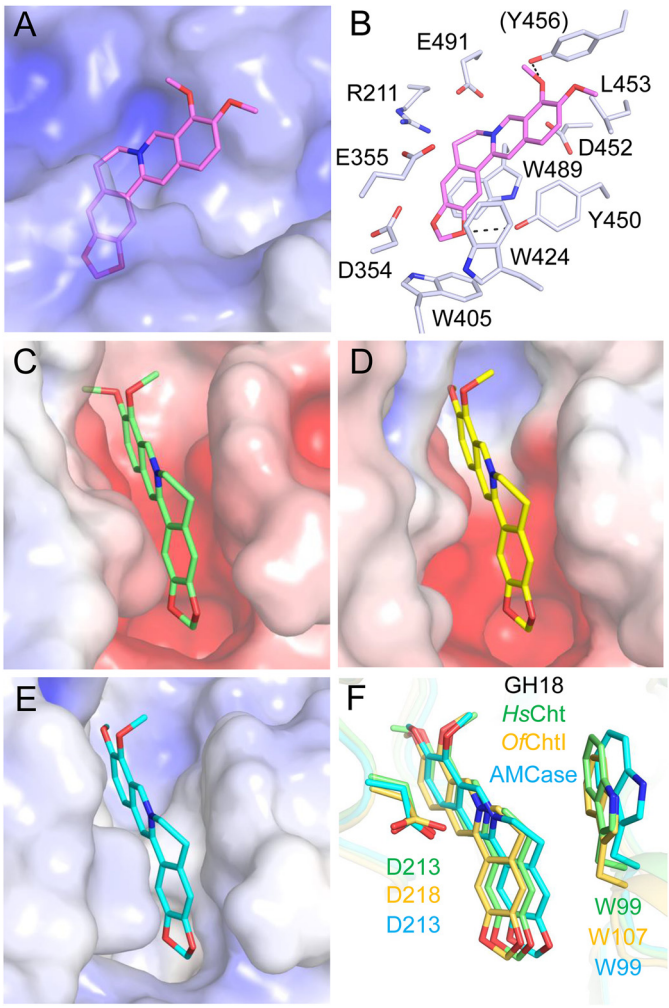

Figure 7. Modeled structures of berberine in complex with GH20 and GH18 enzymes. Electrostatic potential between −6 *kT/e* and 6 *kT/e* was shown as a colored gradient from *red* (acidic) to *blue* (basic). *A*, binding mode of berberine in the active pocket of *Hs*HexB. *B*, locations of the key residues for berberine binding in *Hs*HexB. *C*, binding modes of berberine in the active pocket of *Hs*Cht. *D*, binding modes of berberine in the active pocket of *Of*ChtI. *E*, binding modes of berberine in the active pocket of *AMCase*. *F*, superimposition of the binding modes of berberine with three chitinases. Residues of the *Hs*Cht and its berberine are shown in *green*. Residues of the *Of*ChtI and its berberine are shown in *yellow-orange*. Residues of the AMCase and its berberine are shown in *cyan*.

negatively charged residues (Glu^{57} and Glu^{58} in QacR; Glu^{253} in BmrR; and Asp^{152} in RamR).

The above analysis indicated that the positively charged conjugate plane is important for the binding activities of berberine with target proteins. To find the molecular basis for the selectivity of berberine and its analogs for GH20, GH18, GH84, GH63, and GH13 enzymes, the conformational flexibility and electrostatic potential of these compounds were calculated. As shown in Fig. 11, berberine, thalifendine, and palmatine, which are active against the tested enzymes, have a rigid conjugate plane with a positive charge. By contrast, tetrahydroberberine, which is inactive toward the tested enzymes, has a flexible and neutral structure (less than 3% of tetrahydroberberine is positively charged at pH 6.5 because its pK_a is predicted to be 4.9). These results demonstrated that the positively charged conjugate plane is the core pharmacophore of berberine and should be retained in the further design of berberine-based inhibitors. Additionally, berberine is a good starting point to pursue better affinity or specificity because it can be readily modified at the C8, C13, and O9 sites (3).

Conclusion

In this study, we discovered berberine and its analogs to be inhibitors of GH20, GH18, GH84, and GH63 glycoside hydrolases. By steady inhibition kinetics, X-ray crystallography, and molecular docking, we revealed berberine and its analogs interacted with these enzymes through $\pi-\pi$ stacking or electrostatic interactions. This work not only expands the molecular target library of berberine but also provides a scaffold for developing inhibitors of carbohydrate hydrolyases.

Experimental procedures

Materials

4-Methylumbelliferyl-β-D-GlcNAc (MU-β-GlcNAc), 4-methylumbelliferyl-β-D-*N,N′*-diacetylchitobiose (MU-β-$(GlcNAc)_2$), 4-methylumbelliferyl α-D-glucopyranoside (MU–α-glucose), *Saccharomyces cerevisiae* α-glucosidase I (*Sc*GluI), PPA, amylase activity assay kit, berberine, and palmatine were purchased from Sigma (Shanghai, China). The compound SYSU-1 was synthesized by Ma *et al.* (43) and was kindly provided by Associate Prof. Min Li (Sun Yat-Sen University, China). Thalifendine and tetrahydroberberine were kindly provided by Prof. Xuhong Qian (East China University of Science and Technology, China). The yeast strain *Pichia pastoris* GS115 and the expression vectors pPIC9 and pPIC9K were purchased from Invitrogen (Beijing, China). The chromatographic columns for protein purification were purchased from GE Healthcare. The BCA protein assay kit was purchased from TaKaRa (Dalian, China).

Enzyme preparation

*Of*Hex1 and the mutant *Of*Hex1–W490A were expressed in *P. pastoris* GS115 and purified as described previously with some modifications (52). Briefly, the positive clones were cultured in BMMY broth at 30 °C for 72 h, and methanol (1% of the total volume) was added every 12 h. WT and mutant *Of*Hex1 were purified from the culture supernatant by ammonium sulfate precipitation (65% saturation), followed by affinity chromatography on a HisTrap™ crude column (5 ml).

*Hs*HexB was also expressed in *P. pastoris* GS115. The selected region of the gene encoding *Hs*HexB (GenBank™ accession number NM_000521.3) was synthesized, and a C-terminal His_6 tag was introduced. The DNA fragment was ligated into pPIC9K, and the expression plasmid pPIC9K–*Hs*HexB was transformed into *P. pastoris* GS115 by electroporation. The cells expressing *Hs*HexB were grown in 200 ml of BMGY medium at 30 °C for 24 h and then collected and resuspended in 1 liter of fresh BMMY medium. Methanol was added to a final concentration of 1% (v/v) at 24-h intervals as an inducer. After incubation for an additional 72 h, the supernatant was harvested via centrifugation. *Hs*HexB was purified using immobilized metal ion affinity chromatography with a HisTrap™ crude column (5 ml).

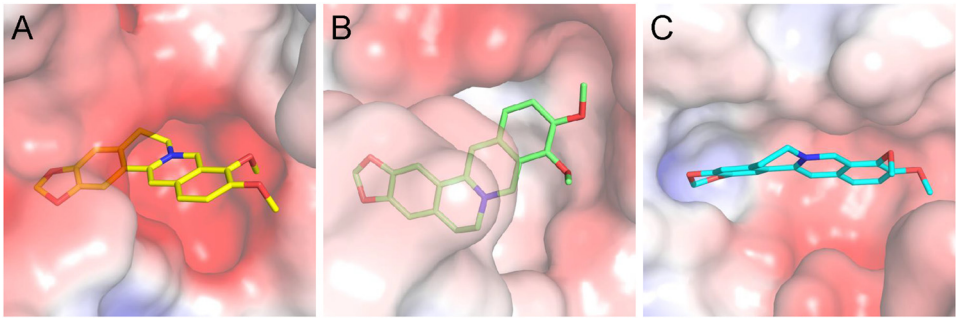

Figure 8. Modeled structures of berberine in complex with GH84, GH63, and GH13 enzymes. Electrostatic potential between −6 *kT/e* and 6 *kT/e* was shown as a colored gradient from *red* (acidic) to *blue* (basic). *A*, binding mode of berberine in the active pocket of *Hs*OGA. *B*, binding modes of berberine in the active pocket of *Sc*GluI. *C*, binding modes of berberine in the active pocket of PPA.

Figure 9. *In vivo* activity of berberine and SYSU-1. *A*, larvae before exposed to the compounds. *B*, larvae of DMSO-fed group 6 days later. *C*, larvae of berberine-fed group 6 days later. *D*, larvae of SYSU-1-fed group 6 days later.

The catalytic domains of *Of*ChtI from *O. furnacalis*, human *Hs*Cht, and human AMCase were expressed in *P. pastoris* GS115 and purified as described previously (39, 53, 54). *Hs*OGA was expressed in *Escherichia coli* and purified as described previously (40). All of the purified proteins were desalted using a HiTrap desalting column (5 ml) with 20 mM bis-tris at pH 6.5 and quantitated using a commercial BCA protein assay kit. The purities of the target proteins were analyzed by SDS-PAGE followed by Coomassie Brilliant Blue R-250 staining.

Inhibitory activity assay

The activities of GH20 Hex and GH84 *Hs*OGA were determined using MU-β-GlcNAc as a substrate. The reaction mixtures used for inhibitor screening consisted of 100 μl of 0.4 nM enzyme, 10 μM MU-β-GlcNAc, 10 μM inhibitors, and 2% DMSO in the buffer (20 mM sodium phosphate, pH 6.5, for *Of*Hex1; 20 mM sodium citrate, pH 4.5, for *Hs*HexB). The reaction in the absence of inhibitors was used as a positive control. After incubating at 30 °C for *Of*Hex1 and 37 °C for *Hs*HexB and *Hs*OGA for an appropriate time, 0.5 M sodium carbonate was added to the reaction mixture, and the fluorescence produced by the released MU was quantified using a Varioskan Flash microplate reader (ThermoFisher Scientific) at excitation and emission wavelengths of 360 and 450 nm, respectively. Experiments were performed in triplicate. For K_i value determination, three substrate concentrations (10, 20, and 40 μM) and varied inhibitor concentrations were used. The K_i values and types of inhibition were determined by linear fitting of the data in Dixon plots.

The activity of GH18 chitinase was determined using MU-β-$(GlcNAc)_2$ as a substrate. The reaction mixtures used for inhibitor screening consisted of 100 μl of 0.4 nM enzyme, 10 μM MU-β-$(GlcNAc)_2$, 10 μM inhibitors, and 2% DMSO in the buffer (20 mM sodium phosphate, pH 6.5, for *Of*ChtI and *Hs*Cht; 20 mM sodium citrate, pH 5.2, for AMCase). The reaction in the absence of inhibitors was used as a positive control. After incubating at 30 °C for *Of*ChtI and 37 °C for *Hs*Cht and AMCase for an appropriate time, 0.5 M sodium carbonate was added to the reaction mixture, and the fluorescence produced by the released MU was quantified as described above. Experiments were performed in triplicate. For K_i value determination, three substrate concentrations (1, 2, and 4 μM for *Of*ChtI and 5, 10, and 20 μM for *Hs*Cht and AMCase) and varied inhibitor concentrations were used. The K_i values and types of inhibition were also determined by linear fitting of the data in Dixon plots

The activity of GH63 *Sc*GluI was determined using MU–α-glucose as a substrate. The reaction mixtures used for inhibitor screening consisted of 100 μl of 0.4 nM enzyme, 10 μM MU–α-glucose, 10 μM inhibitors, and 2% DMSO in the buffer (20 mM sodium phosphate, pH 6.5). The reaction in the absence of inhibitors was used as a positive control. After incubating at 30 °C for an appropriate time, 0.5 M sodium carbonate was added to the reaction mixture, and the fluorescence produced by the released MU was quantified as described above. Experiments were performed in triplicate. For K_i value determination, three substrate concentrations (10, 20, and 40 μM) and varied inhibitor concentrations were used. The K_i values and types of inhibition were also determined by linear fitting of the data in Dixon plots. The activity of GH13 PPA was determined by the amylase activity assay kit according to the manufacturer's instruction.

Protein crystallization and structure determination

Crystallization experiments were performed by the hanging drop–vapor diffusion method at 4 °C. *Of*Hex1 was desalted in 20 mM bis-tris with 20 mM NaCl, pH 6.5, and concentrated to 15.0 mg/ml by ultracentrifugation. The reservoir solution used for crystallization consisted of 100 mM HEPES, pH 6.6–7.5, 100 mM $MgCl_2$, and 26–35% PEG400. Berberine and SYSU-1 were dissolved in the mother liquor with 5% DMSO at 1 mM and soaked into the crystals 1 h before they were transferred to a glycerol solution and flash-cooled in liquid nitrogen.

Diffraction data were collected at the National Center for Protein Science, Shanghai (BL19U1, Pilatus3–6M detector), and processed using HKL2000 (55). The structures of berberine- and SYSU-1-complexed *Of*Hex1 were solved by molecular replacement with PHASER (56) using the structure of unliganded *Of*Hex1 (PDB code 3NSM) as the search model. PHENIX (57) was used for structure refinement. The molecular models were manually built and extended using Coot (58). The stereochemistry of the models was checked by PROCHECK (59). The coordinates of berberine- and SYSU-1-complexed *Of*Hex1 have been deposited under accession codes 5Y0V and 5Y1B. All structural figures were generated using PyMOL (DeLano Scientific LLC, San Carlos, CA). The electrostatic surfaces were calculated using APBS and PDB 2PQR (60–62).

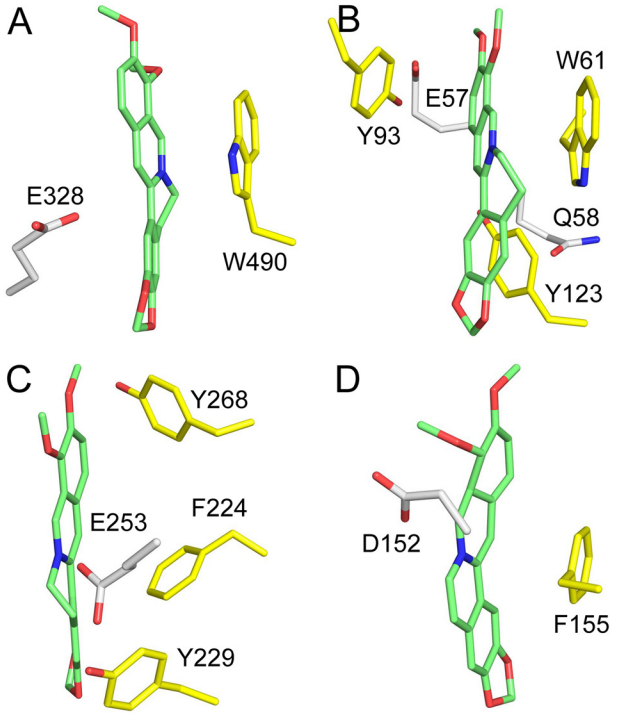

Figure 10. Aromatic residues and negatively charged residues involved in the binding of berberine to *Of*Hex1 (PDB code 5Y0V) (*A*), QacR (PDB code 3BTI) (*B*), BmrR (PDB code 3D6Y) (*C*), and RamR (PDB code 3VW2) (*D*). Berberine is shown in *green*. Aromatic and negatively charged residues are shown in *yellow* and *white*, respectively.

Molecular docking

The PRODRG2 server was used to generate and optimize the initial structure of the compound before docking (63). The molecular docking methodology, performed using AutoDock4.2 software (64, 65), consisted of two steps. First, the protein–ligand complex was obtained by rigid docking and then by flexible docking via setting the active pocket outside ligand-binding residues as flexible. Polar hydrogen atoms and Gasteiger charges were added using AutoDockTools. The center of the grid box was placed at the center of the active pocket of *Hs*HexB (PDB code 1O7A), *Hs*Cht (PDB code 1HKK), *Of*ChtI (PDB code 3WQW), AMCase (PDB code 2YBT), *Hs*OGA (PDB code 5UN9; β-subunit), *Sc*GluI (PDB code 4J5T), and PPA (PDB code 1DHK), and the dimensions of the active site box were set at 50 × 50 × 50 Å, 70 × 70 × 60 Å, 70 × 70 × 70 Å, 60 × 80 × 60 Å, 50 × 50× 60 Å, 90 × 46 × 54 Å, and 50 × 80 × 50 Å. All maps were calculated with a 0.375 Å spacing between the grid points. Docking calculations were carried out using the Lamarckian genetic algorithm, and all parameters were the same for each docking. A population of random individuals (population size: 150), a maximum number of 25,000,000 energy evaluations, and a maximum number of generations of 27,000 were used.

In vivo activity of berberine and SYSU-1

O. furnacalis larvae were fed an artificial diet and reared at 26 ± 1 °C under a 16:8 light/dark photoperiod and 70% relative humidity. Day 1 4th-instar larvae were selected for the feeding experiment. In the experimental groups, an artificial diet containing 0.5 mM compounds (dissolved in DMSO) was used. In the control groups, an artificial diet containing DMSO was

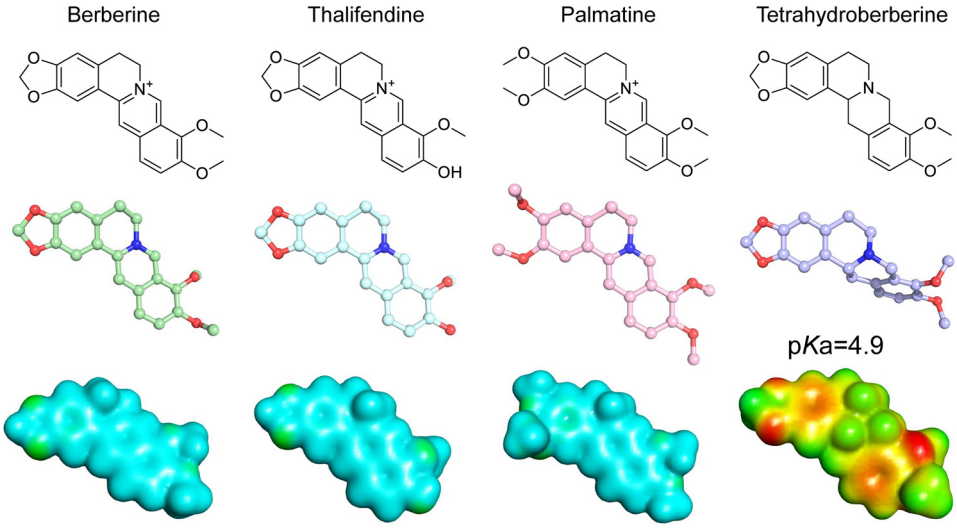

Figure 11. Analysis of the structural characteristics of berberine and its analogs. The energy-minimized structures of berberine and its analogs were generated with MM2 on ChemBio3D (PerkinElmer Life Sciences). The electrostatic potential surfaces for berberine and its analogs were generated with DelPhi on Accelrys Discovery Studio 2016 (Dassault Systèmes). *Red* and *cyan* represent the electronegative and electropositive potentials, respectively, and *green* represents a potential halfway point between the two extremes. The pK_a of tetrahydroberberine was predicted by Marvin Beans (ChemAxon).

used. Each group contained 10 individual larvae and was continuously fed for 7 days. Mortality and developmental defects were recorded every day.

Author contributions—Y. D. and T. D. data curation; Y. D. and Y. Z. software; Y. D., T. L., Y. Z., and T. D. formal analysis; Y. D. and Q. Y. methodology; T. L. and Q. Y. conceptualization; T. L. writing-original draft; T. L. and Q. Y. writing-review and editing; Q. Y. resources; Q. Y. validation; Q. Y. project administration.

Acknowledgments—We thank the staff of BL19U1 beamline at National Center for Protein Sciences Shanghai and Shanghai Synchrotron Radiation Facility, Shanghai, People's Republic of China, for assistance during data collection. We thank Prof. Xuhong Qian (East China University of Science and Technology, Shanghai, China) for providing thalifendine and tetrahydroberberine. We also thank Dr. Min Li (Sun Yat-Sen University, Guangzhou, China) for providing SYSU-1.

References

1. Koehn, F. E., and Carter, G. T. (2005) The evolving role of natural products in drug discovery. *Nat. Rev. Drug Discov.* **4,** 206–220 CrossRef Medline
2. Vuddanda, P. R., Chakraborty, S., and Singh, S. (2010) Berberine: a potential phytochemical with multispectrum therapeutic activities. *Expert Opin. Investig. Drugs* **19,** 1297–1307 CrossRef Medline
3. Singh, I. P., and Mahajan, S. (2013) Berberine and its derivatives: a patent review (2009–2012). *Expert Opin. Ther. Pat.* **23,** 215–231 CrossRef Medline
4. Sun, Y., Xun, K., Wang, Y., and Chen, X. (2009) A systematic review of the anticancer properties of berberine, a natural product from Chinese herbs. *Anticancer Drugs* **20,** 757–769 CrossRef Medline
5. Zhao, H. L., Sui, Y., Qiao, C. F., Yip, K. Y., Leung, R. K., Tsui, S. K., Lee, H. M., Wong, H. K., Zhu, X., Siu, J. J., He, L., Guan, J., Liu, L. Z., Xu, H. X., Tong, P. C., and Chan, J. C. (2012) Sustained antidiabetic effects of a berberine-containing Chinese herbal medicine through regulation of hepatic gene expression. *Diabetes* **61,** 933–943 CrossRef Medline
6. Peng, W. H., Lo, K. L., Lee, Y. H., Hung, T. H., and Lin, Y. C. (2007) Berberine produces antidepressant-like effects in the forced swim test and in the tail suspension test in mice. *Life Sci.* **81,** 933–938 CrossRef Medline
7. Derosa, G., Maffioli, P., and Cicero, A. F. (2012) Berberine on metabolic and cardiovascular risk factors: an analysis from preclinical evidences to clinical trials. *Expert Opin. Biol. Ther.* **12,** 1113–1124 CrossRef Medline
8. Fatehi-Hassanabad, Z., Jafarzadeh, M., Tarhini, A., and Fatehi, M. (2005) The antihypertensive and vasodilator effects of aqueous extract from *Berberis vulgaris* fruit on hypertensive rats. *Phytother. Res.* **19,** 222–225 CrossRef Medline
9. da Silva, A. R., de Andrade Neto, J. B., da Silva, C. R., Campos Rde, S., Costa Silva, R. A., Freitas, D. D., do Nascimento, F. B., de Andrade, L. N., Sampaio, L. S., Grangeiro, T. B., Magalhães, H. I., Cavalcanti, B. C., de Moraes, M. O., and Nobre Júnior, H. V. (2016) Berberine antifungal activity in fluconazole-resistant pathogenic yeasts: action mechanism evaluated by flow cytometry and biofilm growth inhibition in *Candida* spp. *Antimicrob. Agents Chemother.* **60,** 3551–3557 CrossRef Medline
10. Miyazawa, M., Fujioka, J., and Ishikawa, Y. (2002) Insecticidal compounds from *Phellodendron amurense* active against *Drosophila melanogaster*. *J. Sci. Food Agric.* **82,** 830–833 CrossRef
11. Iwasa, K., Moriyasu, M., and Nader, B. (2000) Fungicidal and herbicidal activities of berberine related alkaloids. *Biosci. Biotechnol. Biochem.* **64,** 1998–2000 CrossRef Medline
12. Yu, G., Li, Y., Tian, Q., Liu, R., Wang, Q., Wang, J. Z., and Wang, X. (2011) Berberine attenuates calyculin A-induced cytotoxicity and Tau hyperphosphorylation in HEK293 cells. *J. Alzheimers Dis.* **24,** 525–535 CrossRef Medline
13. Ma, C., Tang, K., Liu, Q., Zhu, R., and Cao, Z. (2013) Calmodulin as a potential target by which berberine induces cell cycle arrest in human hepatoma Bel7402 cells. *Chem. Biol. Drug Des.* **81,** 775–783 CrossRef Medline
14. Peng, P. L., Hsieh, Y. S., Wang, C. J., Hsu, J. L., and Chou, F. P. (2006) Inhibitory effect of berberine on the invasion of human lung cancer cells via decreased productions of urokinase-plasminogen activator and matrix metalloproteinase-2. *Toxicol. Appl. Pharmacol.* **214,** 8–15 CrossRef Medline
15. Jung, H. A., Min, B. S., Yokozawa, T., Lee, J. H., Kim, Y. S., and Choi, J. S. (2009) Anti-Alzheimer and antioxidant activities of *Coptidis rhizoma* alkaloids. *Biol. Pharm. Bull.* **32,** 1433–1438 CrossRef Medline
16. Kong, L. D., Cheng, C. H., and Tan, R. X. (2001) Monoamine oxidase inhibitors from rhizoma of *Coptis chinensis*. *Planta Med.* **67,** 74–76 CrossRef Medline
17. Qin, Y., Pang, J. Y., Chen, W. H., Zhao, Z. Z., Liu, L., and Jiang, Z. H. (2007) Inhibition of DNA topoisomerase I by natural and synthetic mono- and dimeric protoberberine alkaloids. *Chem. Biodivers.* **4,** 481–487 Medline
18. Chai, Y. S., Hu, J., Lei, F., Wang, Y. G., Yuan, Z. Y., Lu, X., Wang, X. P., Du, F., Zhang, D., Xing, D. M., and Du, L. J. (2013) Effect of berberine on cell cycle arrest and cell survival during cerebral ischemia and reperfusion and correlations with p53/cyclin D1 and PI3K/Akt. *Eur. J. Pharmacol.* **708,** 44–55 CrossRef Medline
19. Slámová, K., Bojarová, P., Petrásková, L., and Kren, V. (2010) β-*N*-Acetylhexosaminidase: what's in a name? *Biotechnol. Adv.* **28,** 682–693 CrossRef Medline
20. Liu, T., Duan, Y., and Yang, Q. (2018) Revisiting glycoside hydrolase family 20 β-*N*-acetyl-D-hexosaminidases: crystal structures, physiological substrates and specific inhibitors. *Biotechnol. Adv.* **36,** 1127–1138 CrossRef Medline
21. Liu, T., Zhang, H., Liu, F., Wu, Q., Shen, X., and Yang, Q. (2011) Structural determinants of an insect β-*N*-acetyl-D-hexosaminidase specialized as a chitinolytic enzyme. *J. Biol. Chem.* **286,** 4049–4058 CrossRef Medline
22. Hogenkamp, D. G., Arakane, Y., Kramer, K. J., Muthukrishnan, S., and Beeman, R. W. (2008) Characterization and expression of the β-*N*-acetylhexosaminidase gene family of *Tribolium castaneum*. *Insect Biochem. Mol. Biol.* **38,** 478–489 CrossRef Medline
23. Rong, S., Li, D. Q., Zhang, X. Y., Li, S., Zhu, K. Y., Guo, Y. P., Ma, E. B., and Zhang, J. Z. (2013) RNA interference to reveal roles of β-*N*-acetylglucosaminidase gene during molting process in *Locusta migratoria*. *Insect Sci.* **20,** 109–119 CrossRef Medline
24. Xi, Y., Pan, P. L., and Zhang, C. X. (2015) The β-*N*-acetylhexosaminidase gene family in the brown planthopper, *Nilaparvata lugens*. *Insect Mol. Biol.* **24,** 601–610 CrossRef Medline
25. Zhang, H., Zhao, K., and Fan, D. (2016) Molecular cloning and RNA interference analysis of β-*N*-acetylglucosaminidase in *Mamestra brassicae* L. *J. Asia-Pacif. Entomol.* **19,** 721–728 CrossRef
26. Chen, X., Xu, K., Yan, X., Chen, C., Cao, Y., Wang, Y., Li, C., and Yang, W. (2018) Characterization of a β-*N*-acetylglucosaminidase gene and its involvement in the development of *Lasioderma serricorne* (Fabricius). *J. Stored Prod. Res.* **77,** 156–165 CrossRef
27. Mahuran, D. J. (1999) Biochemical consequences of mutations causing the GM2 gangliosidoses. *Biochim. Biophys. Acta* **1455,** 105–138 CrossRef Medline
28. Liu, J., Shikhman, A. R., Lotz, M. K., and Wong, C. (2001) Hexosaminidase inhibitors as new drug candidates for the therapy of osteoarthritis. *Chem. Biol.* **8,** 701–711 CrossRef Medline
29. Adrangi, S., and Faramarzi, M. A. (2013) From bacteria to human: a journey into the world of chitinases. *Biotechnol. Adv.* **31,** 1786–1795 CrossRef Medline
30. Zhu, Z., Zheng, T., Homer, R. J., Kim, Y. K., Chen, N. Y., Cohn, L., Hamid, Q., and Elias, J. A. (2004) Acidic mammalian chitinase in asthmatic Th2 inflammation and IL-13 pathway activation. *Science* **304,** 1678–1682 CrossRef Medline
31. Wiesner, D. L., Specht, C. A., Lee, C. K., Smith, K. D., Mukaremera, L., Lee, S. T., Lee, C. G., Elias, J. A., Nielsen, J. N., Boulware, D. R., Bohjanen, P. R., Jenkins, M. K., Levitz, S. M., and Nielsen, K. (2015) Chitin recognition via chitotriosidase promotes pathologic type-2 helper T cell responses to cryptococcal infection. *PLoS Pathog.* **11,** e1004701 CrossRef Medline

32. Van Dyken, S. J., Liang, H. E., Naikawadi, R. P., Woodruff, P. G., Wolters, P. J., Erle, D. J., and Locksley, R. M. (2017) Spontaneous chitin accumulation in airways and age-related fibrotic lung disease. *Cell* **169,** 497–509.e13 CrossRef Medline
33. Kim, L. K., Morita, R., Kobayashi, Y., Eisenbarth, S. C., Lee, C. G., Elias, J., Eynon, E. E., and Flavell, R. A. (2015) AMCase is a crucial regulator of type 2 immune responses to inhaled house dust mites. *Proc. Natl. Acad. Sci. U.S.A.* **112,** E2891–E2899 CrossRef Medline
34. Wu, Y., Egerton, G., Underwood, A. P., Sakuda, S., and Bianco, A. E. (2001) Expression and secretion of a larval-specific chitinase (family 18 glycosyl hydrolase) by the infective stages of the parasitic nematode, *Onchocerca volvulus*. *J. Biol. Chem.* **276,** 42557–42564 CrossRef Medline
35. Vinetz, J. M., Dave, S. K., Specht, C. A., Brameld, K. A., Xu, B., Hayward, R., and Fidock, D. A. (1999) The chitinase PfCHT1 from the human malaria parasite *Plasmodium falciparum* lacks proenzyme and chitin-binding domains and displays unique substrate preferences. *Proc. Natl. Acad. Sci. U.S.A.* **96,** 14061–14066 CrossRef Medline
36. Horsch, M., Mayer, C., Sennhauser, U., and Rast, D. M. (1997) β-*N*-Acetylhexosaminidase: a target for the design of antifungal agents. *Pharmacol. Ther.* **76,** 187–218 CrossRef Medline
37. Qian, X., Lee, P. W., and Cao, S. (2010) China: forward to the green pesticides via a basic research program. *J. Agric. Food Chem.* **58,** 2613–2623 CrossRef Medline
38. Andersen, O. A., Dixon, M. J., Eggleston, I. M., and van Aalten, D. M. (2005) Natural product family 18 chitinase inhibitors. *Nat. Prod. Rep.* **22,** 563–579 CrossRef Medline
39. Jiang, X., Kumar, A., Liu, T., Zhang, K. Y., and Yang, Q. (2016) A novel scaffold for developing specific or broad-spectrum chitinase inhibitors. *J. Chem. Inf. Model.* **56,** 2413–2420 CrossRef Medline
40. Li, B., Li, H., Lu, L., and Jiang, J. (2017) Structures of human *O*-GlcNAcase and its complexes reveal a new substrate recognition mode. *Nat. Struct. Mol. Biol.* **24,** 362–369 CrossRef Medline
41. Barker, M. K., and Rose, D. R. (2013) Specificity of processing α-glucosidase I is guided by the substrate conformation: crystallographic and *in silico* studies. *J. Biol. Chem.* **288,** 13563–13574 CrossRef Medline
42. Liu, T., Guo, P., Zhou, Y., Wang, J., Chen, L., Yang, H., Qian, X., and Yang, Q. (2014) A crystal structure-guided rational design switching non-carbohydrate inhibitors' specificity between two β-GlcNAcase homologs. *Sci. Rep.* **4,** 6188 Medline
43. Ma, Y., Ou, T. M., Tan, J. H., Hou, J. Q., Huang, S. L., Gu, L. Q., and Huang, Z. S. (2009) Synthesis and evaluation of 9-*O*-substituted berberine derivatives containing aza-aromatic terminal group as highly selective telomeric G-quadruplex stabilizing ligands. *Bioorg. Med. Chem. Lett.* **19,** 3414–3417 CrossRef Medline
44. Yang, Y., Liu, T., Yang, Y., Wu, Q., Yang, Q., and Yu, B. (2011) Synthesis, evaluation, and mechanism of *N,N,N*-trimethyl-D-glucosamine-(1→4)-chitooligosaccharides as selective inhibitors of glycosyl hydrolase family 20 β-*N*-acetyl-D-hexosaminidases. *ChemBioChem* **12,** 457–467 CrossRef Medline
45. Liu, T., Zhang, H., Liu, F., Chen, L., Shen, X., and Yang, Q. (2011) Active-pocket size differentiating insectile from bacterial chitinolytic β-*N*-acetyl-D-hexosaminidases. *Biochem. J.* **438,** 467–474 CrossRef Medline
46. Liu, T., Xia, M., Zhang, H., Zhou, H., Wang, J., Shen, X., and Yang, Q. (2015) Exploring NAG-thiazoline and its derivatives as inhibitors of chitinolytic β-acetylglucosaminidases. *FEBS Lett.* **589,** 110–116 CrossRef Medline
47. Maier, T., Strater, N., Schuette, C. G., Klingenstein, R., Sandhoff, K., and Saenger, W. (2003) The X-ray crystal structure of human β-hexosaminidase B provides new insights into Sandhoff disease. *J. Mol. Biol.* **328,** 669–681 CrossRef Medline
48. Williams, L. K., Zhang, X., Caner, S., Tysoe, C., Nguyen, N. T., Wicki, J., Williams, D. E., Coleman, J., McNeill, J. H., Yuen, V., Andersen, R. J., Withers, S. G., and Brayer, G. D. (2015) The amylase inhibitor montbretin A reveals a new glycosidase inhibition motif. *Nat. Chem. Biol.* **11,** 691–696 CrossRef Medline
49. Peters, K. M., Schuman, J. T., Skurray, R. A., Brown, M. H., Brennan, R. G., and Schumacher, M. A. (2008) QacR-cation recognition is mediated by a redundancy of residues capable of charge neutralization. *Biochemistry* **47,** 8122–8129 CrossRef Medline
50. Newberry, K. J., Huffman, J. L., Miller, M. C., Vazquez-Laslop, N., Neyfakh, A. A., and Brennan, R. G. (2008) Structures of BmrR-drug complexes reveal a rigid multidrug binding pocket and transcription activation through tyrosine expulsion. *J. Biol. Chem.* **283,** 26795–26804 CrossRef Medline
51. Yamasaki, S., Nikaido, E., Nakashima, R., Sakurai, K., Fujiwara, D., Fujii, I., and Nishino, K. (2013) The crystal structure of multidrug-resistance regulator RamR with multiple drugs. *Nat. Commun.* **4,** 2078 CrossRef Medline
52. Liu, T., Liu, F., Yang, Q., and Yang, J. (2009) Expression, purification and characterization of the chitinolytic β-*N*-acetyl-D-hexosaminidase from the insect *Ostrinia furnacalis*. *Protein Expr. Purif.* **68,** 99–103 CrossRef Medline
53. Chen, L., Zhou, Y., Qu, M., Zhao, Y., and Yang, Q. (2014) Fully deacetylated chitooligosaccharides act as efficient glycoside hydrolase family 18 chitinase inhibitors. *J. Biol. Chem.* **289,** 17932–17940 CrossRef Medline
54. Sutherland, T. E., Andersen, O. A., Betou, M., Eggleston, I. M., Maizels, R. M., van Aalten, D., and Allen, J. E. (2011) Analyzing airway inflammation with chemical biology: dissection of acidic mammalian chitinase function with a selective drug-like inhibitor. *Chem. Biol.* **18,** 569–579 CrossRef Medline
55. Otwinowski, Z., and Minor, W. (1997) Processing of X-ray diffraction data collected in oscillation mode. *Methods Enzymol.* **276,** 307–326 CrossRef Medline
56. McCoy, A. J. (2007) Solving structures of protein complexes by molecular replacement with Phaser. *Acta Crystallogr. D Biol. Crystallogr.* **63,** 32–41 CrossRef Medline
57. Adams, P. D., Afonine, P. V., Bunkóczi, G., Chen, V. B., Davis, I. W., Echols, N., Headd, J. J., Hung, L. W., Kapral, G. J., Grosse-Kunstleve, R. W., McCoy, A. J., Moriarty, N. W., Oeffner, R., Read, R. J., Richardson, D. C., *et al.* (2010) PHENIX: a comprehensive Python-based system for macromolecular structure solution. *Acta Crystallogr. D Biol. Crystallogr.* **66,** 213–221 CrossRef Medline
58. Emsley, P., Lohkamp, B., Scott, W. G., and Cowtan, K. (2010) Features and development of Coot. *Acta Crystallogr. D Biol. Crystallogr.* **66,** 486–501 CrossRef Medline
59. Laskowski, R. A., Macarthur, M. W., Moss, D. S., and Thornton, J. M. (1993) Procheck–a program to check the stereochemical quality of protein structures. *J. Appl. Crystallogr.* **26,** 283–291 CrossRef
60. Baker, N. A., Sept, D., Joseph, S., Holst, M. J., and McCammon, J. A. (2001) Electrostatics of nanosystems: application to microtubules and the ribosome. *Proc. Natl. Acad. Sci. U.S.A.* **98,** 10037–10041 CrossRef Medline
61. Dolinsky, T. J., Nielsen, J. E., McCammon, J. A., and Baker, N. A. (2004) PDB2PQR: an automated pipeline for the setup of Poisson-Boltzmann electrostatics calculations. *Nucleic Acids Res.* **32,** W665–W667 CrossRef Medline
62. Unni, S., Huang, Y., Hanson, R. M., Tobias, M., Krishnan, S., Li, W. W., Nielsen, J. E., and Baker, N. A. (2011) Web servers and services for electrostatics calculations with APBS and PDB2PQR. *J. Comput. Chem.* **32,** 1488–1491 CrossRef Medline
63. Schüttelkopf, A. W., and van Aalten, D. M. (2004) PRODRG: a tool for high-throughput crystallography of protein-ligand complexes. *Acta Crystallogr. D Biol. Crystallogr.* **60,** 1355–1363 CrossRef Medline
64. Morris, G. M., Goodsell, D. S., Halliday, R. S., Huey, R., Hart, W. E., Belew, R. K., and Olson, A. J. (1998) Automated docking using a Lamarckian genetic algorithm and an empirical binding free energy function. *J. Comput. Chem.* **19,** 1639–1662 CrossRef
65. Morris, G. M., Huey, R., Lindstrom, W., Sanner, M. F., Belew, R. K., Goodsell, D. S., and Olson, A. J. (2009) AutoDock4 and AutoDockTools4: automated docking with selective receptor flexibility. *J. Comput. Chem.* **30,** 2785–2791 CrossRef Medline